Ionic Current Rectification, Breakdown, and Switching in Heterogeneous Oxide Nanofluidic Devices

Li-Jing Cheng* and L. Jay Guo*

Department of Electrical Engineering and Computer Science, The University of Michigan, Ann Arbor, Michigan 48109

ARTICLE

ABSTRACT We investigate several ion transport behaviors in sub-20 nm nanofluidic channels consisting of heterogeneous oxide materials. By utilizing distinct isoelectric points of SiO_2 and Al_2O_3 surfaces and photolithography to define the charge distribution, nanofluidic channels containing positively and negatively charged surfaces are created to form an abrupt junction. This method provides much more robust surface charges than previous approaches by surface chemical treatment. The fabricated nanofluidic diodes exhibit high rectification of ion current and achieve record-high rectification factors (ratio of forward current to reverse current) of over 300. The current—voltage property of the device follows the theoretical model quantitatively, except that at low ion concentrations the forward current degrades and the reverse current is greater than theoretical prediction, which can be attributed to access resistance and breakdown of water molecules. The breakdown effect characterized by a negative conductance followed by a rapid increase of current is observed in a double junction diode. The occurrence of the breakdown is found to be enhanced by the abruptness of the junction between the heterogeneous nanochannels. Finally, we demonstrate ionic switching in a three-terminal nanofluidic triode in which the ionic flow can be electrically regulated between different channel branches. The study provides insight into the ion transport behavior in nanofluidic devices containing heterogeneous surfaces.

KEYWORDS: nanofluidics · heterogeneous nanochannels · ionic rectification · water dissociation · nanofluidic diode · nanofluidic triode · ionic switch

A nanofluidic device exhibiting ion current rectifying behavior is of great interest because it provides a basis to control the ion flow in the channel. Ionic current rectification can be generated in a nanofluidic channel that contains asymmetric distribution of cation—anion concentration ratios (or equivalently, asymmetric Donnan potentials).[1] The asymmetric cation—anion ratio along the channel produces asymmetric electrostatic impact of the surface charges on the ions at the two ends of channel. Depending on the polarity of the applied electric field, the uneven ion flows from the two ends lead to either accumulation or depletion of ions in the nanochannel and, as a result, either enhance or reduce the ionic conductance. The cation—anion ratio in a nanochannel is determined by the bath ion concentration, the size of channel, and the polarity and density of the channel surface charge. Accordingly, to generate the ionic rectification effect in a nanofluidic device, imbalanced cation—anion ratios can be established by controlling these three parameters at the two ends of the channel. For example, homogeneous silica nanochannels containing an ion concentration gradient produce asymmetric electrostatic impact on the ions at the two channel ends by asymmetric ion concentrations[1] and conical nanopores by asymmetric geometry.[2−4] Nanofluidic diodes or bipolar membranes utilize the asymmetric (*i.e.*, opposite) polarity of fixed charges to achieve the same effect. The idea of a nanofluidic diode consisting of opposite polarity of surface charges on either half of the nanochannel was proposed by Daiguji and co-workers to produce rectification of ion current.[5] The fundamental of this device structure is essentially the same as the widely studied bipolar membranes in electrochemistry. It is known that bipolar membranes, composed of a negatively charged cation exchange membrane and a positively charged anion exchange membrane, present ion rectification[6] and have been used for decades in many applications such as electrodialysis and chemical separation.[7,8] Possessing similar properties but much smaller size and structure regularity, nanofluidic diodes may be integrated on a microfluidic chip to perform pH control and a chemical separation process.[9,10]

One of the key challenges to producing nanofluidic diodes is to create asymmetric surface charges along a nanochannel. Karnik and co-workers developed diffusion-limited patterning (DLP) to pattern the cationic protein avidin inside biotinylated nanofluidic channels to modify the surface charge of the nanochannel.[11]

*Address correspondence to chenglj@gmail.com, guo@eecs.umich.edu.

Received for review November 10, 2008 and accepted January 29, 2009.

Published online February 16, 2009.
10.1021/nn8007542 CCC: $40.75

© 2009 American Chemical Society

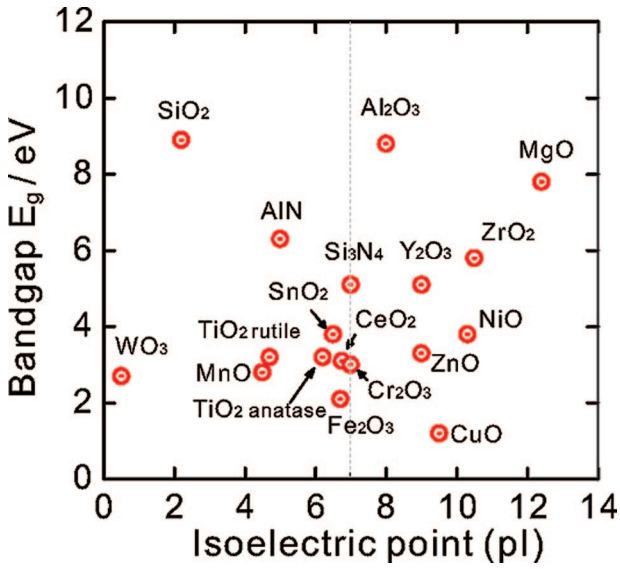

Figure 1. Summarized isoelectric point (pI) *versus* energy band gap (E_g) data of different solid oxides and nitrides. The data may vary depending on the preparation methods.

Heterogeneous surface charge distribution along the nanochannels was achieved by introducing avidin from one of the channel openings until half of the biotinylated nanochannel was covered with the avidin protein molecules.[12] Since the avidin coated and biotinylated surfaces contain positive and neutral surface charges, respectively, the surface charge discontinuity is created in the nanochannels. Moreover, Vlassiouk *et al.* reported a nanofluidic diode created by modifying the surface chemistry of the conical nanopores in PET membranes.[13] The surface of the nanopore has one half covered by carboxyl groups and the other half by amino groups. The dependence of the rectifying behavior on the pH values and electrolyte concentrations were studied.

The limitations of the surface chemical modification approach described above are twofold: (1) the proteins used have finite sizes and could change the nanochannel dimension and may interfere with other molecules in the nanochannel; and (2) such surface charge preparation is time-consuming and not robust enough such that it can only be used close to the ambient temperature environment. To overcome these limitations, we developed a technique to create asymmetric surface charge distributions by using two solid state oxide materials of different isoelectric points, that is, a negatively charged silicon dioxide nanochannel and a positively charged Al_2O_3 nanochannel connected in series. The solid oxide nanofluidic diode relies on the arrangement of these oxide materials using microfabrication technology without chemical treatments. We have demonstrated this principle by constructing the first solid oxide heterogeneous nanofluidic devices using nickel oxide and silicon dioxide.[14] In this paper, we will provide details on the qualification of solid oxides for heterogides foreneous nanofluidic devices and their electrical properties. Apart from the ion current rectification in forward bias configuration, we report the observation of breakdown effect in a reverse biased nanofluidic double junction diode similar to that in a semiconductor pnp diode, and we attribute this effect to the splitting of water molecules to ions. Last, we demonstrate ionic current regulation using a three-terminal nanofluidic triode.

Solid Oxide Materials for Nanofluidic Devices. Solid state oxide materials possessing electrically insulating property and hydrophilic surface are our candidate materials for constructing solid state nanofluidic channels. The channel structure is of necessity an insulator; otherwise, additional shunt current paths through the conductive channel walls would develop under an applied voltage bias. Most transition-metal oxides are relatively easily reduced to form semiconducting or metallic phases because the lower part of the conduction band originates from the d rather than s orbital, resulting in lower energy band gap. Other than oxides, silicon nitride is one of the widely used insulating materials in microfabrication. However, its hydrophobic surface does not qualify for nanofluidic applications without an additional oxidation process. Generally speaking, solid oxide surfaces are electrically charged in aqueous suspension; thereupon, they associate with water molecules through charge−dipole interaction resulting in hydrophilicity. Positive or negative surface sites can be developed on the surface of solids in contact with aqueous solutions. In the case of oxide or hydroxide surfaces, these sites are protonated or deprotonated following the equilibrium $-MO + H^+ \leftrightarrow -MOH^+$ or $-MO^- + H^+ \leftrightarrow -MOH$, where $-MO$ denotes a surface oxide group.[15,16] The protonation−deprotonation reaction is pH dependent. As the pH increases, the equilibrium shifts to the left, resulting in less positive charges or more negative charges, whereas at lower pH values, it becomes more positive. There exists a certain pH value defined as isoelectric point (pI) at which the amount of positive surface charge equals that of negative charge, yielding no net charge. The data of isoelectric point (pI) *versus* energy band gap for various oxide materials collected from prior literature[16,17] are summarized in Figure 1. The values of each material may vary with their methods of preparation. Among these solid oxides, non-transition-metal oxides such as SiO_2, Al_2O_3, and MgO are preferred because they have larger energy band gaps (8−10 eV); moreover, they have pI values deviating from 7, which can be utilized to produce different surface charges in aqueous suspension at physiological pH range. NiO was also selected for our study because of its positive surface charge, moderate high band gap (about 3.9 eV), and the compatibility to the standard microfabrication process. MgO can become hydroxylated upon exposure to H_2O. The adsorption of water results in the formation of $MgOH^+$ or $Mg(OH)_2$, which yields an isoelectric point (pI) of about 12. Other metal

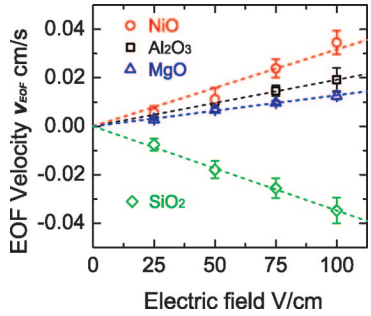

Figure 2. Electroosmotic flow velocities corresponding to various applied electric fields in the microfluidic chambers made of different oxide surfaces at [KCl] = 1 mM.

oxides such as Al_2O_3 surfaces also produce positive charge in water suspension and have a pI of ~8. Silica SiO_2 surfaces acquire a negatively charged SiO^- state when in contact with water by the dissociation of silanol groups, and its pI is about 2−3. Similar to the electrostatic interaction in the acid dissociation process, the strength of the oxyacids in the surface −MOH groups depends on the size and the charge of the metal cations. It has been reported that pI roughly varies linearly with the ratio of ionic charge (Z) to solid oxide ionic radius ($R = 2r_o + r_+$), Z/R, where r_o and r_+ are oxygen and cation radii, respectively. Isoelectric point increases as Z/R decreases.[15] A surface −MO group with smaller radius R tends to deprotonate, leaving negative charges and therefore has lower pI. Take MgO, Al_2O_3, and SiO_2, for example, in terms of the solid oxide radii, R, they have the relationship of $SiO_2 < Al_2O_3 < MgO$. Likewise, their pI values show a similar relationship (Figure 1). On the other hand, NiO has a similar high pI to MgO because the lattice constant of NiO (4.18 Å in (100)) is very close to that of MgO (4.21 Å in (100)).[17]

With given pH values of the environment, the surface charge polarity of the metal oxides can be recognized directly from their pI values, but their surface charge density needs to be determined by separate means. We estimated the effective surface charge densities and polarities of SiO_2, MgO, Al_2O_3, and NiO by measuring electroosmotic mobilities in microchannels made of these oxide materials as shown in Figure 2 (details can be found in Methods), where the surface charge density is related to the electroosmotic mobility *via* zeta-potential according to an approximated formula

$$\sigma_{eff} = \sqrt{8\varepsilon_0\varepsilon_r kTn_b}\ \sinh(q\zeta / 2kT)$$

TABLE 1. Summarized Electroosmotic Mobility, μ_{eo}, ζ-Potentials, and Effective Surface Charges, σ_{eff}, Deduced from EOF Experiment at [KCl] = 1 mM

	SiO_2	Al_2O_3	MgO	NiO
μ_{eo} ($cm^2/V \cdot s$)	−0.0348	0.0192	0.0128	0.0317
ζ (mV)	−49.1	27.1	18.0	44.8
σ_{eff} (mC/m^2)	−4.24	2.10	1.36	3.77

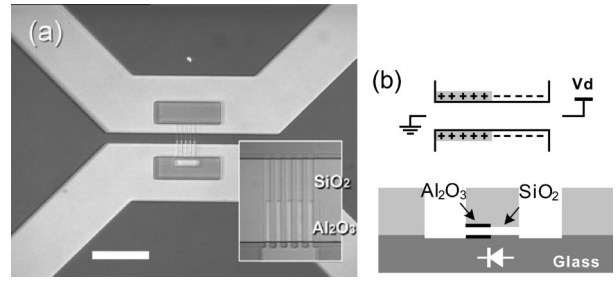

Figure 3. (a) Microscope image and (b) schematic of a heterogeneous nanochannel consisting of two different oxide surfaces. The heterogeneous oxide nanochannel connects between two 20 μm deep PDMS microfluidic channels. The inset in (a) is a magnified image showing that the lower half of the nanochannel is wrapped by Al_2O_3 and the top half by SiO_2 surfaces. The scale bar is 100 μm. For the measurement, a voltage bias, V_d, is connected to the negatively charged SiO_2 channel, and the positively charged Al_2O_3 channel is grounded.

where $\varepsilon_0\varepsilon_r$, ζ, and n_b are permittivity, zeta-potential, and the number density of ions in the bulk solution, respectively.[18]

As summarized in Table 1, our measurement showed that the effective surface charges on these oxide materials are all on the same order of magnitude (1 to 5 mC/m^2). The surface charge densities of SiO_2 and Al_2O_3 obtained by zeta-potential measurement are close to those evaluated from the ion conductance in the nanochannels made of these materials (*i.e.*, 4.4 and 1.3 mC/m^2 for SiO_2 and Al_2O_3, respectively; see Supporting Information for more details). By employing different solid oxides having distinct pI values in a nanofluidic device, we can tailor surface charge distributions in the nanochannel. The way to fabricate heterogeneous nanochannels is similar to that reported in our previous work on SiO_2 nanochannels, which is based on a sub-20 nm thick sacrificial layer approach to precisely define the height of the nanochannel.[1] The difference here is that two additional Al_2O_3 thin films were patterned by photolithography to sandwich half of the sacrificial layer in order to form a sub-20 nm thick nanochannel comprising two sections made of different oxide surfaces (Figure 3). Details about the fabrication process are described in the Methods.

Experimental and Theoretical Studies of an Alumina−Silica Nanofluidic Diode. The current−voltage ($I-V$) characteristics of the $SiO_2-Al_2O_3$ nanofluidic diode were measured at varied bath KCl concentrations ranging from 10 μM to 1 M. In the measurement, as illustrated in Figure 3b, a voltage bias V_d was applied to the bath next to the SiO_2 nanochannel, while the Al_2O_3 side was grounded. The experimental $I-V$ curves are presented in Figure 4a−f (red empty circles). It is shown that the $I-V$ characteristics display strong rectification effect at every concentration except at 1 M. Figure 4g summarizes the channel conductances under the biases of 1 and −1 V (blue and red symbols) obtained at varied bath concentrations and the associated rectifying factors (shaded bars), which is defined as the ratio of forward bias cur-

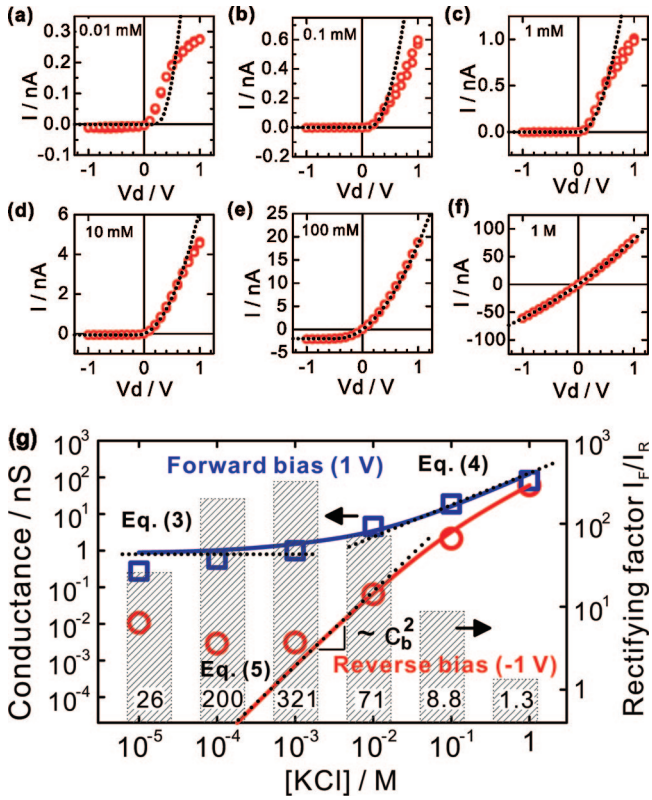

Figure 4. *I*−*V* characteristics of a nanofluidic diode (equivalent channel width = 2.5 μm × 10) measured at different bath KCl concentrations: (a) 0.01 mM, (b) 0.1 mM, (c) 1 mM, (d) 10 mM, (e) 100 mM, and (f) 1 M. The red symbols are experimental data, and the black dashed curves are the calculated result based on a simplified 1D transport model (discussed below). (g) Log−log plot of the experimental forward conductances at 1 V (blue squares), reverse conductances at −1 V (red circles), and the rectifying factors (shaded bars) at different bath concentrations. The rectifying factor is defined by I_F/I_R under the bias of 1 or −1 V at different bath concentrations. The solid blue and red curves are the theoretical conductances calculated by 2D PNP equations, having very close results acquired from eq 1) or the simplified eqs 3−5 under certain conditions.

rent to reverse bias current under the biases of 1 and −1 V. The rectifying factor reaches its maximum, 321, when the bath KCl concentration is 1 mM. It is also important to note that the rectifying factor can be even greater under higher voltage biases. To our knowledge, this is the highest rectification ratio reported in literature for nanofluidic channel devices. We found that above 1 mM the rectifying factor degrades significantly with the increase of concentration. Below 1 mM, the rectifying factors decrease with ion concentration but are still relatively high: about 200 for 0.1 mM and decreases to 30 for 0.01 mM. Such high rectification behavior was not observed in the prior works.[12−14] In addition to the heterogeneity of the surface charge distributed along the nanochannel forming a positive−negative (p−n) junction, we attribute the result to the abruptness of the p−n junction well-defined by photolithography, which can hardly be achieved by surface chemistry modification *via* diffusion. Such an abrupt junction yields a more efficient control of ion accumulation and depletion in the nanochannel.

To show a clear view of the reverse bias currents, all the *I*−*V* curves are summarized in a semilog graph in Figure 5a. It can be seen that both reverse bias currents and forward bias currents increase with bath concentrations, especially above 1 mM concentration. However, the experimental *I*−*V* curves with ion concentrations below 1 mM are close to each other as compared with those above 1 mM. In this low concentration regime, different bath concentrations do not alter channel conductance significantly. The resulting independence between the ion conductance and the bath concentrations takes place under a similar condition in which the surface charge governs ion transport. It occurs when the bath concentration is less than half of fixed charge density[19] ($c_b < f/2$ with $f = 2\sigma_s/qN_Ah$, where σ_s and h are the surface charge density and the height of nanochannels; q and N_A are charge and Avogadro's number; $f/2 \approx 2$ mM for $\sigma_s = 4$ mC/m^2 and $h = 20$ nm) or if the electric double layer (EDL) overlaps in the nanochannel. With the corresponding Debye length of 9.6 nm, the 1 mM KCl concentration is the critical condition that yields the EDL overlap in the 20 nm thick nanofluidic channel.

To better understand how the ion current level varies with bath concentrations as well as how the current depends on voltage, we developed a simplified 1D *I*−*V* model to investigate the current−voltage relationship. This 1D model was derived from the Nernst−Planck equation and taking into account electroneutrality. The model was verified by the solutions calculated from 2D Poisson−Nernst−Planck (PNP) equations.[1,14] To simplify the calculation but without losing generality, the model assumes that the device made of SiO_2 and Al_2O_3 nanochannels has equal length L and fixed charge density f ($=2\sigma_s/(qN_Ah)$) but with opposite signs. The bath concentration, c_b, in both sides is equal. More details on the derivation of the equation

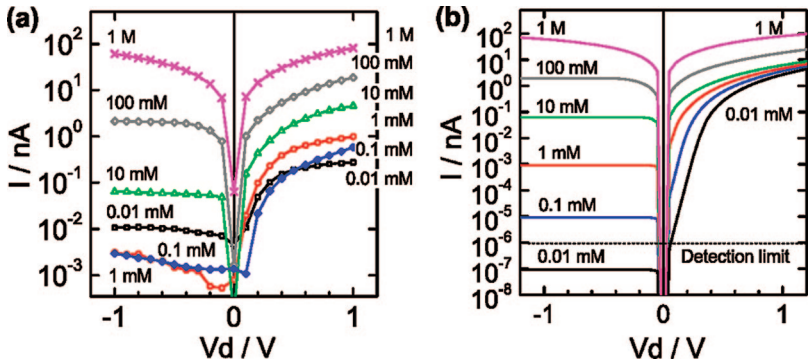

Figure 5. Summarized experimental *I*−*V* curves (a) and simplified 1D *I*−*V* model (b) of a nanofluidic diode in a semilog graph to show the reverse bias currents in more detail. The theoretical rectifying factors in (b) for various KCl concentrations from 0.01 mM to 1 M are 4.75×10^6, 1.47×10^5, 2.54×10^3, 101, 9.4, and 1.3. Note that the currents shown here are absolute values.

can be found in the Supporting Information. The dashed lines in Figure 4a−f represent the $I-V$ curves calculated from the simplified 1D equation:

$$\frac{F}{RT}V_d = 2\sinh^{-1}\left(\frac{f}{2c_b}\right) - 2\coth^{-1}\sqrt{1+(2c_b/f)^2+2JL/fFD} + 2\left(-\sqrt{1+(2c_b/f)^2} + \sqrt{1+(2c_b/f)^2+2JL/fFD}\right) \quad (1)$$

where F is the Faraday number and J is the current density responding to the applied voltage V_d; the diffusion coefficients of cations and anions are assumed to be the same D.[20] The first and second terms of the equation are contributed by the Donnan potentials across the channel entrances and the junction of the heterogeneous channels, respectively, while the last term is derived from the sum of the voltage drops on the positive and negative nanochannels. Except for some minor difference in the mathematical forms, eq 1 is basically identical to the one reported in some other literature to describe the $I-V$ relation of bipolar membranes.[21,22] The simplified $I-V$ model has the following features:

(1) At large forward biases, the equation approximates to

$$J_F = J(V_d \gg 0) = DF\frac{f}{8L}\left(4\sqrt{1+(2c_b/f)^2}\frac{F}{RT}V_d + \left(\frac{F}{RT}V_d\right)^2\right) \quad (2)$$

(2) At low bath ion concentrations ($c_b \ll f/2$), the forward current is proportional to the fixed charge density f of the nanochannels but independent of bath ion concentrations c_b.

$$J_F(c_b \ll f/2) = DF\frac{f}{2L}\left(\frac{F}{RT}V_d + \frac{1}{4}\left(\frac{F}{RT}V_d\right)^2\right) \quad (3)$$

Equation 3 agrees with the experimental observation that at small c_b ($<f/2$, *i.e.*, 2 mM), the ion conductance does not change much with c_b.

(3) At high bath ion concentrations ($c_b \gg f/2$), both f and c_b affect the forward ion current density giving the relation

$$J_F(c_b \gg f/2) = DF\frac{1}{L}\left(c_b\frac{F}{RT}V_d + \frac{f}{8}\left(\frac{F}{RT}V_d\right)^2\right) \quad (4)$$

However, because of the high c_b, if V_d is not so large, eq 4 reduces to a linear form, independent of fixed charge density f, $J_F(c_b \gg f/2) = (DF^2/LRT)c_bV_d$.

Equations 2−4 suggest that, in the forward conduction regime, the current is a quadratic function of the forward bias, which has also been identified in the previous literature.[5] In another case, if the fixed charge density f is large enough that the concentration of the minority ions in the nanochannel is negligible, the current and applied voltage can have an exponential relationship as in the case of semiconductor devices and some ion exchange membranes.[23,24]

Under reverse biases ($V_d \ll 0$), the second term of eq 1, that is, the junction voltage, dominates the total voltage. As a result, the current saturates to

$$J_{sat} = -\frac{2D}{fL}c_b^2 \quad (5)$$

The saturation current is proportional to the square of the bath concentration and inversely proportional to the fixed charge density of the nanochannels. It is worthwhile to point out that the reverse ion current in the nanochannels can reach saturation for all bath concentrations. However, for a high bath concentration, such as 1 M concentration in Figure 4f, a much larger reverse bias is required to deplete the ions at the channel junction. Theoretically, with eqs 2 and 5, the rectifying factor can be obtained by J_F/J_{sat}, yielding a function inversely proportional to c_b^2; nevertheless, it is invalid to apply the equation to this case (*e.g.*, Figure 4f), in which the device does not attain saturation at the reverse bias of interest.

By carefully selecting the fixed charge density f in eq 1, the 1D $I-V$ model fits well to the experimental data, especially for the cases of high bath concentration (Figure 4d−f,g). At high KCl concentration, the rectification factor is lower because the amount of mobile ions is high enough to shield the surface charges and hence weakens their impact on the channel conductance. By fitting the channel conductance measured at 1 M KCl, we can estimate the size of the channel to be about 14−17 nm, consistent with the channel height as determined by the SEM microscopy, and the surface charge density about 7−12 mC/m^2, which is greater than the value estimated from the zeta-potential measurement and the ion conductance characterizations of homogeneous nanochannels but still within a reasonable range. At low c_b, it can be seen in Figure 4a−c that the experimental forward currents match the model at lower forward biases; however, they deviate from the model further as c_b decreases more from 1 mM. The ion conductance reduces as the apply voltage increases. The result has been proved to be the consequence of the access resistance produced by the heterogeneous channel entrance which has positively charged Al_2O_3 channel sitting next to the negatively charged SiO_2 bath side walls. Such heterogeneous channel entrance functions as a parasitic diode connecting in series to the original p−n junction. When the device is forward biased, the parasitic diode at the Al_2O_3 channel entrance is, however, reversed biased, leading to a high series resistance. Due to its open geometry, the parasitic diode at the entrance is weaker in controlling the ions than the p−n junction in the nanochannel does. As a result, it reveals crucial impact only under high forward bias

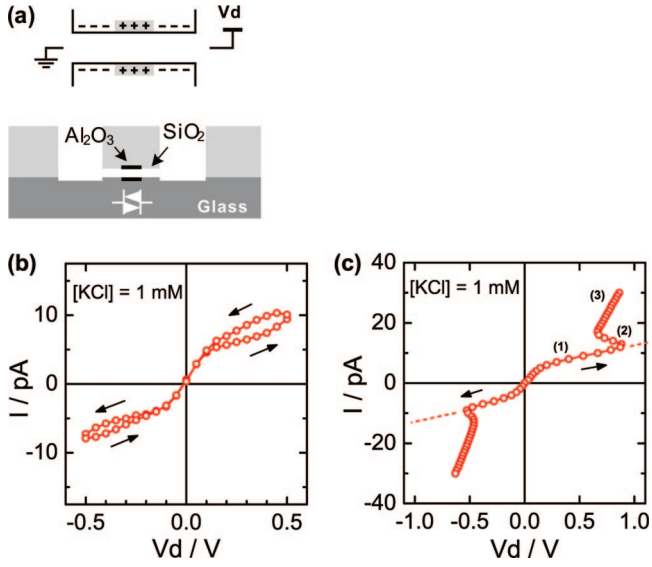

Figure 6. (a) Schematic of a nanofluidic diac consisting of $SiO_2-Al_2O_3-SiO_2$ nanochannels. Each segment is 20 μm long, 2.5 μm × 5 wide. *I*−*V* characteristic of the device with 1 mM of KCl concentration measured by sweeping voltage and acquiring current (b), and by sweeping current and acquiring voltage (c), with the arrows indicating the sweeping directions. Three conduction regimes are observed in (b): (1) saturation regime, (2) negative-resistance regime, and (3) breakdown regime. The dashed lines extending from regime (1) are the anticipated *I*−*V* behavior.

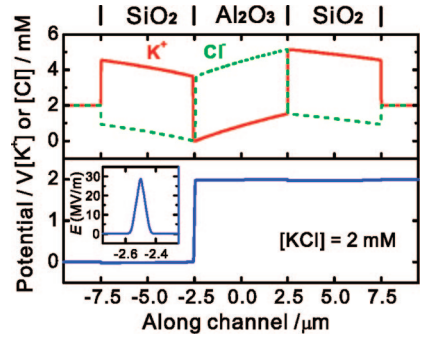

Figure 7. Ion concentration distributions and potential profiles calculated by 2D PNP equations in a 20 nm thick nanofluidic diac filled with 2 mM KCl solution in both sides under the bias of $V_d = 2$ V. The surface charge densities of SiO_2 and Al_2O_3 are −4 and 4 mC/m^2, respectively. Each segment of the heterogeneous nanochannel is 5 μm long. Inset shows the absolute value of the electric field distribution near the depletion junction with the peak ~30 MV/m at $x = -2.5$ μm.

(for the p−n junction) or at low bath concentrations. Details about the entrance effect will be discussed in another paper.

Similar to the trend of the experimental data (Figure 5a), the *I*−*V* model (Figure 5b) shows that the current levels at the +1 V bias are close to each other at different low bath concentrations and increase significantly when $c_b > 1$ mM. The phenomenon can be described by eq 3 that at low c_b the forward current is governed only by the fixed charge densities *f* of the nanochannels; however, at higher c_b, the bath ion concentration starts to play a role as formulated in eq 4 because the fixed charges lose its control on the ions in the nanochannels. In the case of reverse bias, both the experimental and calculated reverse currents saturate; nevertheless, as the bath concentrations reduce below 1 mM, the reverse current does not decrease consistently. Instead, they stop around 1−10 pA, which is still 2 to 3 orders of magnitude above the current detection limit of the measurement instrument (Agilent 4156). The agreement between experimental (Figure 4g) and the theoretical rectifying factors in Figure 5b restricts to high c_b. The deviation at low concentrations indicates an additional factor contributing to the reverse bias ion current. Yielding a similar result from the 1D *I*−*V* model, the theoretical conductances under the biases of ±1 V obtained by solving 2D PNP equations (blue and red solid curves in Figure 4g) show the forward conductance decreases with bath concentrations and saturates at low concentration. The reverse conductances (red solid curve) decrease with bath concentration by a power of 2 when $c_b < 10$ mM, which agrees with the saturation current described in eq 5.

Breakdown Effect in a Silica−Alumina−Silica Nanofluidic Diac. In the previous section, we characterized the *I*−*V* behavior of a nanofluidic p−n diode and found that at low ion concentration regime the reverse currents do not reduce with c_b as predicated by both 1D *I*−*V* model and 2D PNP model. In addition, it was found that the reverse currents measured by sweeping the voltage back and forth tend to show hysteresis even at a slow rate (>2 s for each data point) as shown in Figure 4a, which was not encountered in measuring forward currents. The discrepancy implies an ion transport phenomenon different from the theoretical model and inspires us to study the reverse bias current in heterogeneous nanochannels. Here we test a double junction diode in the form of a $SiO_2-Al_2O_3-SiO_2$ nanochannel with equal length of 20 μm in each segment, as illustrated in Figure 6a. Having similar characteristics of a semiconductor pnp diode (or diac, as named after *di*ode for *a*lternating *c*urrent), the nanofluidic pnp diode has been proposed theoretically[5] and demonstrated experimentally[25] to have its current saturating under both positive and negative biases. The result is the consequence of the fact that either polarity of the applied bias can cause one of the two pn junctions reverse biased and hence saturates the ion current. It can be seen in the ion concentration and potential profiles calculated using 2D PNP equations (Figure 7) that almost all the applied voltage drops across the reverse biased p−n junction, yielding a high electric field in a restricted space. The use of the pnp diode provides the advantages that it has two pn junctions for observation and there exists no heterogeneous entrance edge effect as mentioned above. The *I*−*V* curve of a pnp diode measured by sweeping the voltage forward and backward is shown in Figure 6b. Two hysteresis loops can be seen in the saturation regimes. The finding motivated us to check

if there is more than one current state for each voltage bias. By sweeping the current and acquiring the voltage, a distinctive breakdown behavior was observed in the $I-V$ curve in Figure 6c, which resembles the DC behavior of a semiconductor diac.[26] This $I-V$ characteristic is composed by three regimes: (1) saturation regime, (2) negative-resistance regime, and (3) breakdown regime. The saturation regime and breakdown regime show a large difference in channel conductance and are about 8.1 and 92.7 pS, respectively. The negative-resistance regime can disappear after a high-current, long-term operation, but the breakdown was found to be reproducible as long as the current level is not too high. Similar breakdown behaviors in ionic devices have been studied in the field-enhanced water dissociation in bipolar ion-exchange membranes[7,8,22,24,27] or the punch-through in biological membranes.[28] The punch-through behavior tends to take place in thin membranes that are few tens of nanometers thick and therefore is not likely the case in our 60 μm long nanochannels because it requires a much larger voltage to deplete all the K and Cl ions in the nanochannels. Therefore, we ascribe the drastic increase of ion currents in the breakdown regime (segment (3) of the $I-V$ curve in Figure 6c) to the dissociation of water molecules to positive hydroniums and negative hydroxyl ions under the high electric field at a reverse biased junction (*e.g.*, the left $SiO_2-Al_2O_3$ junction of Figure 7). As the applied voltage crosses a critical voltage bias, turning up this additional current source, the voltage required to sustain the original saturation current (segment (1)) drops abruptly, resulting in a negative-resistance regime (segment (2)). Under a reverse bias $V_d = 2$ V, the thickness of the space charge region at an abrupt junction is in the range of 80 nm, estimated by[26,28,29]

$$W_D = \sqrt{2\varepsilon_0\varepsilon_r(\Psi_{D,j} + V_d)(f_P^{-1} + f_N^{-1}) \times 10^{-3} / qN_A}$$

where ε_r, ε_o, and $\Psi_{D,j}$ are dielectric constant of the solution, permittivity of free space, and the Donnan potential of the junction, while f_P and f_N are the fixed charge densities of the Al_2O_3 and SiO_2 nanochannels with the value of about 4 mM for $\sigma_s = 4$ mC/m^2 and $h = 20$ nm. The resulting electric field across this region ($E = V_d/W_D$) is about 2×10^7 V/m, which is close to the result solved by 2D PNP equations, as shown in the inset of Figure 7. With the high electric field and the induced lowering of water's dielectric constant, the water dissociation constant can increase according to second Wien effect.[22,30] Correspondingly, a similar breakdown effect is known in a nonheavily doped semiconductor pn junction, where the behavior represented by a sudden increase in the reverse current is caused by the electron−hole pair generation through impact ionization under high electric field.[26] It is worth pointing out

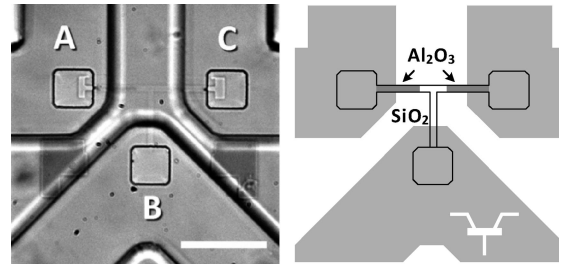

Figure 8. Microscopic image and the corresponding schematics of a nanofluidic triode, which is a three-terminal double junction nanofluidic device composed by Al_2O_3 and SiO_2 nanochannels, connecting to three separate PDMS microchannels (rendered as the gray areas in the schematics). The scale bar in the microscopic image is 50 μm.

that not every heterogeneous nanochannel exhibits apparent breakdown effect. We found that the alignment accuracy of the top and bottom Al_2O_3 patterns during device fabrication may affect whether the breakdown behavior can be observed. The misalignment of the two patterns creates a gradual junction having SiO_2 and Al_2O_3 surfaces overlapped instead of an abrupt boundary. As a result, the electric field at the junction is significantly weakened at reverse bias. For example, a 1 μm misalignment results in a 10-fold reduction of the electric field at the reverse biased junction to 10^6 V/m (*i.e.*, 1 V/1 μm). This may explain why the previously reported nanofluidic diodes built by chemical modification of surface charge did not show such breakdown behavior because of the difficulty in creating abrupt junction by the diffusion process.[12,13]

Finally, we found that both the nanofluidic pn diode and the pnp double junction diode can degrade under a long-term, high-current measurement. After high voltage measurement ($V_d > 5$ V) at low bath concentration ($c_b < 10$ mM) for more than 5 min, the pn junction device can lose its rectification capability, and sometimes this process is not reversible. The degradation is hypothesized to result from the change of surface charge density due to the high current stressing, or the significant change of the solution's pH value arose from water dissociation at high reverse biases. Further investigation is required to delineate the cause.

Ionic Switching in a Nanofluidic Triode. Now that we can precisely define the negatively charged SiO_2 nanochannels and positively charged Al_2O_3 nanochannels on a substrate, it is possible to build nanofluidic devices or networks to regulate ion transport with more functionalities. Here we demonstrate an ionic switching device

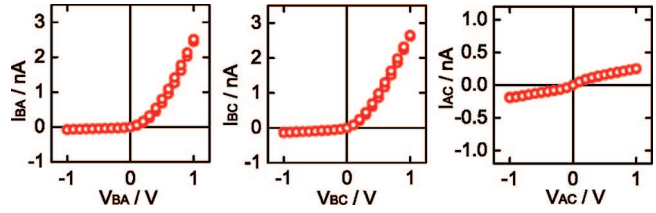

Figure 9. $I-V$ characteristics of the nanofluidic triode measured across every two terminals with a KCl concentration of 50 mM.

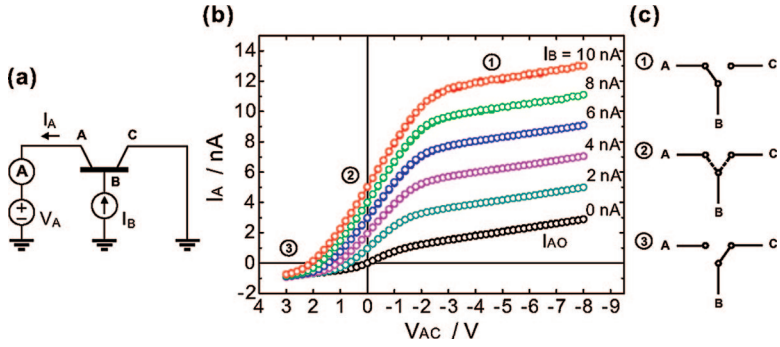

Figure 10. (a) Schematic of a nanofluidic triode operated as an ionic switch. (b) $I_A - V_{AC}$ relationships of the device with varied I_B under a KCl concentration of 50 mM. (c) Switching conditions at corresponding operation regimes indicated in (b).

implemented by the proposed technology. Figure 8 is a microscopic image of a three-terminal double junction nanofluidic device, an npn triode, composed by a SiO_2 nanochannel sandwiched by two Al_2O_3 nanochannels. Unlike the aforementioned nanofluidic diac, this triode device has the SiO_2 nanochannel in the middle branching out to an additional microchannel. The $I-V$ characteristics measured between every two terminals with 50 mM KCl concentration shown in Figure 9 indicate that between microchannel A and B is a nanofluidic diode as it appears between microchannel B and C, while the channel across A and C having a low ion conductance is an npn diac. The rectification factors of the two diodes are greater than 30. Because the device is characterized under a relatively high KCl concentration, the access resistance effect due to the heterogeneous channel entrance in a forward biased diode and the water dissociation effect in a reverse biased diac were not observed.

The nanofluidic triode can be used as a switch for the regulation of ion flow. Consider a circuit built by the nanofluidic triode in Figure 10a; the nanofluidic triode is biased to produce a constant ionic current I_B flowing through the terminal B. By adjusting the corresponding voltage bias across A and C, V_{AC}, the ionic current I_B can be directed to terminal A or C serving as a single-pole, double-throw switch as illustrated in Figure 10c. Figure 10b relates the ion current flowing out of terminal A, I_A, and the applied voltage V_{AC} at varied I_B values. When terminal B is open ($I_B = 0$), the measured I_A is essentially a diac behavior which can be treated as a current, I_{AO}, leaking across two junctions from terminal C to A. The leakage current I_{AO} here is relatively high because the high ion concentration we used makes it difficult to turn off one of the junctions at reverse bias. Otherwise, I_{AO} can be reduced to a few pA by lowering the ion concentrations, as shown in the diac in Figure 6, or by increasing the surface charge density in nanochannels. It was found that with a given positive ion current I_B the ion currents I_A saturate to a high current level when biased at a large negative V_{AC}. In this regime (1), the nanofluidic junction between terminals A and B turns on whereas the other side turns off. The ion current at terminal A is contributed by the entire ion current I_B migrating from B along with the leakage current I_{AO} from C (*i.e.*, $I_A = I_B + I_{AO}$). When V_{AC} shifts from negative to positive, the AB junction turns off while the BC junction turns on. In this transition regime (2), there exists a range of bias in which both junctions slightly turn on. For instance, at zero V_{AC}, I_B can flow to both terminals A and C with equal amount leading to $I_A = I_B/2$. In regime (3), a large positive V_{AC} bias turns off the AB junction but turns on the BC junction. I_B flows to terminal C. What was measured in terminal A is just the leakage current I_{AO} flowing from A to C regardless of different I_B applied into the device. The nanofluidic triode device can be operated in such a way that the direction of ion flow is switchable at a channel intersection. Such function requires two-dimensional nanofluidic networks which can hardly be achieved in nanopore-based devices.

The demonstration of the nanofluidic switch inspires us to consider the possibility of creating a nanofluidic bipolar junction transistor (BJT) which is a three-terminal device similar to the proposed structure but has a short base area (the middle section of the device) to amplify the input I_B current (*i.e.*, $I_A/I_B \gg 1$). In a semiconductor BJT, the base region must be made shorter than the carriers' (electrons or holes) diffusion length, so that they can diffuse across it in much less time than the semiconductor's minority carrier lifetime to minimize the percentage of carriers recombining before reaching the other junction. Unlike the electron−hole system in semiconductor materials, cations and anions do not recombine (except protons and hydroxide ions). Therefore, when a nanofluidic pn junction is forward biased, both ions can accumulate at the pn junction, significantly larger than the background concentrations at equilibrium, resulting in the domination of drift current. Because of the dissimilar ion transport mechanisms, the nanofluidic triode should operate in a different way to resemble the function of a semiconductor BJT. The nanofluidic triode can, for example, have the AB junction forward biased whereas the BC junction is reverse biased such that the cation current injecting from terminal A migrates fast enough across the middle base section toward terminal C to reduce the possibility of being caught by the electric field from terminal B. The way it operates is essentially more close to the function of a vacuum tube triode. This device behavior, however, may be hardly achieved in an ionic system because the mobility of ions in electrolyte solutions is very low, about 7 orders of magnitude less than that of the electrons or holes in semiconducting materials. Such low mobility makes it difficult for a nanofluidic device to realize the same function with comparable device dimensions.

CONCLUSION

In summary, we have demonstrated high ionic rectification in a nanofluidic pn diode composed by heterogeneous oxide surfaces. Standard semiconductor processing method provides precise definition of oxide patterns and sharp heterogeneous oxide junctions. The experimental results match the theoretical models, except for some deviations at low ion concentrations. The unanticipated depression of forward conductance is caused by a heterogeneous channel entrance effect, which will be analyzed in detail in a separate paper. The reverse current underestimated by the theoretical calculation is likely related to the breakdown current in reverse bias. The breakdown current was clearly demonstrated in a pnp nanofluidic diode that shows a direct parallel to the semiconductor counterpart. More studies are needed to unravel the relation between the breakdown current and surmised water splitting effect. Furthermore, regulation of ionic flow has been implemented in a three-terminal heterogeneous nanofluidic triode. We demonstrated that, by controlling the applied biases, ionic currents can be switched to the designated channel branches. On the basis of the proposed technology and the theoretical model we developed, nanofluidic networks with more sophisticated functionalities can be built to precisely control the transport of ions or charged molecules, providing key functions for bio/chemical separation and reaction in an integrated micro/nanoscale system.

METHODS

Silicon oxide (SiO_2) and aluminum oxide (Al_2O_3) are the two oxide materials chosen to make heterogeneous nanofluidic devices because they produce opposite surface charge polarities in aqueous suspension. To make a nanochannel having both Al_2O_3 and SiO_2 surfaces, a 5 nm thick Al_2O_3 thin film was first deposited and patterned on a glass substrate to function as its bottom surface by photolithography, e-beam evaporation, and lift-off process. An amorphous silicon sacrificial layer was then deposited on top by sputtering and patterned into multiple parallel 2.5 μm wide channels. The a-Si layer was 20 nm thick, which will determine the height of nanochannels. To form the Al_2O_3 ceiling of the nanochannel, the same process was applied on top of the a-Si channel patterns after removing its native oxide by dilute HF. The removal of the native SiO_2 on the a-Si sacrificial layer was found essential to prevent the Al_2O_3 surface from being blocked by a SiO_2 layer after the formation of the nanochannels. The use of dilute HF can slightly etch the a-Si sacrificial layer and therefore make the Al_2O_3 nanochannels slightly thinner than expected. The Al_2O_3 patterns on the top and bottom of the nanochannels had the same geometry and were well aligned. A 5 μm thick PECVD oxide was deposited at 200 °C on top of the sample to form the SiO_2 channel surface as well as the physical structure of the device. To form contact holes, we etched several holes through the PECVD oxide layer and the Al_2O_3 layer by high density C_2F_6/Ar plasma etch until the a-Si sacrificial layer was exposed. After removing the photoresist, O_2 plasma and C_2F_6/Ar plasma were used to remove photoresist residuals and the oxidized a-Si surfaces to facilitate the following removal of the sacrificial layer. XeF_2 etch was performed to remove a-Si sacrificial layers, resulting in void nanochannel structures. A PDMS microfluidic channel was aligned and bonded on the nanofluidic device with thin uncured PDMS as a glue layer to form an excellent sealing. After curing at 65 °C for 4 h and an O_2 plasma treatment, the device is ready for testing. Depending on the desired device properties, the Al_2O_3 can be replaced by other materials, such as NiO or MgO.

Acknowledgment. This work was supported by a Riethmiller Fellowship and NSFC Grant No. 60528003.

Supporting Information Available: Estimation of surface charge density by electroosmosis and nanochannel conductance; current−voltage characterization and current stability; derivation of the simplified 1D $I-V$ model. This material is available free of charge *via* the Internet at http://pubs.acs.org.

REFERENCES AND NOTES

1. Cheng, L. J.; Guo, L. J. Rectified Ion Transport Through Concentration Gradient in Homogeneous Silica Nanochannels. *Nano Lett.* **2007**, *7*, 3165–3171.
2. Siwy, Z.; Gu, Y.; Spohr, H. A.; Baur, D.; Wolf-Reber, A.; Spohr, R.; Apel, P.; Korchev, Y. E. Rectification and Voltage Gating of Ion Currents in a Nanofabricated Pore. *Europhys. Lett.* **2002**, *60*, 349–355.
3. Siwy, Z.; Heins, E.; Harrell, C. C.; Kohli, P.; Martin, C. R. Conical-Nanotube Ion-Current Rectifiers: The Role of Surface Charge. *J. Am. Chem. Soc.* **2004**, *126*, 10850–10851.
4. Siwy, Z. S. Ion-Current Rectification in Nanopores and Nanotubes with Broken Symmetry. *Adv. Funct. Mater.* **2006**, *16*, 735–746.
5. Daiguji, H.; Oka, Y.; Shirono, K. Nanofluidic Diode and Bipolar Transistor. *Nano Lett.* **2005**, *5*, 2274–2280.
6. Lovrecek, B.; Despic, A.; Bockris, J. O. M. Electrolytic Junctions with Rectifying Properties. *J. Phys. Chem.* **1959**, *63*, 750–751.
7. Mani, K. N. Electrodialysis Water Splitting Technology. *J. Membr. Sci.* **1991**, *58*, 117–138.
8. Simons, R.; Khanarian, G. Water Dissociation in Bipolar Membranes: Experiments and Theory. *J. Membr. Biol.* **1978**, *38*, 11–30.
9. Nagarale, R. K.; Gohil, G. S.; Shahi, V. K. Recent Developments on Ion-Exchange Membranes and Electromembrane Processes. *Adv. Colloid Interface Sci.* **2006**, *119*, 97–130.
10. Gao, M. T.; Hirata, M.; Koide, M.; Takanashi, H.; Hano, T. Production of L-Lactic Acid by Electrodialysis Fermentation (EDF). *Process Biochem.* **2004**, *39*, 1903–1907.
11. Karnik, R.; Castelino, K.; Duan, C. H.; Majumdar, A. Diffusion-Limited Patterning of Molecules in Nanofluidic Channels. *Nano Lett.* **2006**, *6*, 1735–1740.
12. Karnik, R.; Duan, C. H.; Castelino, K.; Daiguji, H.; Majumdar, A. Rectification of Ionic Current in a Nanofluidic Diode. *Nano Lett.* **2007**, *7*, 547–551.
13. Vlassiouk, I.; Siwy, Z. S. Nanofluidic Diode. *Nano Lett.* **2007**, *7*, 552–556.
14. Cheng, L. J.; J., G. L. Ionic Rectifying Effect in Bipolar Nanochannels. *MicroTAS* **2007**, 979–981.
15. Parks, G. A. Isoelectric Points of Solid Oxides Solid Hydroxides and Aqueous Hydroxo Complex Systems. *Chem. Rev.* **1965**, *65*, 177–198.
16. Bourikas, K.; Kordulis, C.; Lycourghiotis, A. Differential Potentiometric Titration: Development of a Methodology for Determining the Point of Zero Charge of Metal (Hydr)oxides by One Titration Curve. *Environ. Sci. Technol.* **2005**, *39*, 4100–4108.
17. Henrich, V. E.; Cox, P. A. *The Surface Science of Metal Oxides*; Cambridge University Press: Cambridge, 1994.
18. Kirby, B. J.; Hasselbrink, E. F. Zeta Potential of Microfluidic Substrates: 1. Theory, Experimental Techniques, and Effects on Separations. *Electrophoresis* **2004**, *25*, 187–202.
19. Stein, D.; Kruithof, M.; Dekker, C. Surface-Charge-Governed Ion Transport in Nanofluidic Channels. *Phys. Rev. Lett.* **2004**, *93*, 1–4.

20. The ion diffusion coefficients of K and Cl ions are close: $D_K = 1.94 \times 10^{-9}$ m^2/s, $D_{Cl} = 2.01 \times 10^{-9}$ m^2/s.
21. Sokirko, A. V.; Ramirez, P.; Manzanares, J. A.; Mafe, S. Modeling of Forward and Reverse Bias Conditions in Bipolar Membranes. *PCCP* **1993**, *97*, 1040–1049.
22. Mafe, S.; Ramirez, P. Electrochemical Characterization of Polymer Ion-Exchange Bipolar Membranes. *Acta Polym.* **1997**, *48*, 234–250.
23. Sonin, A. A.; Grossman, G. Ion-Transport through Layered Ion-Exchange Membranes. *J. Phys. Chem.* **1972**, *76*, 3996–4006.
24. Bassignana, I. C.; Reiss, H. Ion-Transport and Water Dissociation in Bipolar Ion-Exchange Membranes. *J. Membr. Sci.* **1983**, *15*, 27–41.
25. Kalman, E. B.; Vlassiouk, I.; Siwy, Z. S. Nanofluidic Bipolar Transistors. *Adv. Mater.* **2008**, *20*, 293–297.
26. Sze, S. M. *Physics of Semiconductor Devices*; John Wiley & Sons: New York, 1981.
27. Grossman, G. Water Dissociation Effects in Ion-Transport Through Composite Membrane. *J. Phys. Chem.* **1976**, *80*, 1616–1625.
28. Coster, H. G. L. A Quantitative Analysis of Voltage−Current Relationships of Fixed Charge Membranes and Associated Property of Punch-Through. *Biophys. J.* **1965**, *5*, 669–686.
29. Mafe Mafe, S.; Manzanares, J. A.; Ramirez, P. Model for Ion-Transport in Bipolar Membranes. *Phys. Rev. A* **1990**, *42*, 6245–6248.
30. Onsager, L. Deviations from Ohm's Law in Weak Electrolytes. *J. Chem. Phys.* **1934**, *2*, 599–615.